Technical Report Documentation Page

1. Report No.	2. Government Accession No.	3. Recipient's Catalog No.
jahs2274		

4. Title and Subtitle	5. Report Date
Helicopter Noise Source Separation Using an Order Tracking Filter	August 2023
	6. Performing Organization Code

7. Author(s)	8. Performing Organization Report No.
Joel Sundar Rachaprolu & Eric Greenwood	

9. Performing Organization Name and Address	10. Work Unit No. (TRAIS)
Center of Excellence for: Alternative Jet Fuels and Environment Penn State University, University Park, PA	11. Contract or Grant No. 13-C-AJFE-PSU-067

12. Sponsoring Agency Name and Address	13. Type of Report and Period Covered
Federal Aviation Administration Office of Environment and Energy	Journal Article
	14. Sponsoring Agency Code

15. Supplementary Notes

16. Abstract

Due to the importance of understanding the aeroacoustics of rotorcraft with continually changing noise sources, this paper presents a new technique for source separation from ground-based acoustic measurements. The source separation process is based on combining a time-domain de-Dopplerization method with the Vold–Kalman order tracking filter approach. This process can extract rotor harmonic noise even when the sources are continuously changing with time, including impulsive events such as blade–vortex interaction noise. The advantage of this approach over traditional methods such as harmonic averaging is that the phase and amplitude relationship of acoustic signals is preserved throughout the extraction process. The approach is applied to the measured acoustic data from a Bell 430 helicopter. The measured data were separated into main rotor harmonic, tail rotor harmonic, and broadband residual components. For steady-state conditions, the extracted components could be depropagated to form acoustic hemispheres showing the directivity of the separated main and tail rotor components. The source separation process was also applied to a maneuvering flight condition. Each component has different pulse shapes and directivity trends, consistent with aeroacoustic theory.

17. Key Words	18. Distribution Statement
ASCENT	

19. Security Classif. (of this report)	20. Security Classif. (of this page)	21. No. of Pages	22. Price
Unclassified	Unclassified		

Helicopter Noise Source Separation Using an Order Tracking Filter

Joel Sundar Rachaprolu*
Graduate Research Assistant

Eric Greenwood
Assistant Professor

Department of Aerospace Engineering, Penn State University
University Park, PA

Due to the importance of understanding the aeroacoustics of rotorcraft with continually changing noise sources, this paper presents a new technique for source separation from ground-based acoustic measurements. The source separation process is based on combining a time-domain de-Dopplerization method with the Vold–Kalman order tracking filter approach. This process can extract rotor harmonic noise even when the sources are continuously changing with time, including impulsive events such as blade–vortex interaction noise. The advantage of this approach over traditional methods such as harmonic averaging is that the phase and amplitude relationship of acoustic signals is preserved throughout the extraction process. The approach is applied to the measured acoustic data from a Bell 430 helicopter. The measured data were separated into main rotor harmonic, tail rotor harmonic, and broadband residual components. For steady-state conditions, the extracted components could be depropagated to form acoustic hemispheres showing the directivity of the separated main and tail rotor components. The source separation process was also applied to a maneuvering flight condition. Each component has different pulse shapes and directivity trends, consistent with aeroacoustic theory.

Nomenclature

A	complex pressure amplitude, Pa
a_0	speed of sound, m/s
bw	bandwidth, Hz
k	order number
P	complex phasor
p	acoustic pressure, Pa
q	Vold–Kalman (V-K) filter order
r	distance, m
t	observer time, s
w	V-K weighting factor
x	deterministic/harmonic part of signal, Pa
y	measured signal, Pa
v	nondeterministic/broadband part of signal, Pa
τ	emission time, s
ω	shaft speed, rev/s

Introduction

Among the many barriers to the use of rotorcraft in residential and urban areas is the noise generated during low-altitude operations. To overcome this problem, the first step is to understand the physical mechanisms of rotor noise generation. This understanding can then be used to develop viable ways of reducing the noise impact using a range of methods, either through design changes or by tailoring flight operations to avoid noisy operating conditions. Since rotor noise is sensitive to changes in the operating condition, the noise of helicopters is highly variable, with the prominence of different mechanisms varying continuously and resulting in fluctuations in the radiated noise. The noise of multirotor unmanned aerial systems (UAS) and advanced air mobility (AAM) is expected to be even more variable, as these vehicles often use rotational speed variation as a part of their flight control systems. Additionally, the aerodynamic and acoustic interactions between the multiple rotors are likely to have a large effect on the noise radiation of the vehicle.

Rotor noise sources can be divided into harmonic and broadband components. Harmonic noise is from sources such as thickness noise, lower harmonic loading noise, and unsteady loading due to aerodynamic interactions such as blade–vortex interaction (BVI). Due to its impulsive nature, BVI tends to dominate noise metrics when it occurs (Ref. 1). Because it is governed by the aerodynamic interactions of the rotor with its own wake, it is highly sensitive to variations in the rotor operating state, giving rise to variable noise that fluctuates from one blade passage period to the next. This is especially true during maneuvering flight when the rotor quickly passes through a wide range of operating conditions. For most conventional helicopters, the lower harmonic loading and thickness noise of the tail rotor occurs in the same frequency range, making it difficult to distinguish the relative contributions of the two noise sources for

*Corresponding author; email: joelsundar@gmail.com.
Presented at the Vertical Flight Society' 78th Annual Forum & Technology Display, Ft. Worth, TX, May 10–12, 2022. Manuscript received November 2022; accepted August 2023.

any given flight condition. There can also be aerodynamic interactions between the main and tail rotor that result in another source of interaction noise, sometimes described as "burble" (Ref. 2). In addition to the tonal noise components, there can be significant broadband noise generated in the same range of frequencies; effective extraction of the tonal components from the signal can allow for a more detailed examination of the remaining broadband noise. However, this "residual" signal will still contain some components related to the harmonic noise sources if fluctuations in the harmonic noise are not accounted for in the extraction technique.

Developing a complete understanding of how the different physical mechanisms of noise generation contribute to measured acoustic signals will require data analysis techniques that can separate the fluctuating noise components. For helicopters, separation of the main and tail rotor components from the acoustic signal will help to isolate the harmonic and broadband noise sources, evaluate their relative importance for a particular flight condition, and to understand the physical mechanisms that govern noise generation. Moreover, if the extraction can be done in the time domain, that is, the phase relations of the components are not discarded a range of data-processing techniques in the time and frequency domains can be used to analyze the extracted results.

Background

Rotor harmonic averaging has often been applied to wind tunnel measurements of rotor noise to reduce the variability of the data and separate the harmonic and broadband components from each other (Ref. 1). This method works by dividing the recorded pressure time-history signal into windows associated with each complete rotation of the rotor shaft. These windows are then ensemble averaged in the time domain, extracting the signal component that is purely harmonic with the shaft order. This technique requires that the rotor be acoustically stationary. Fluctuations in the amplitude and phase of the tonal noise, for instance, due to the effect of turbulence on the rotor wake (Ref. 3), are not extracted by the harmonic averaging process. Similar techniques have been applied to separate the main rotor and tail rotor noise components from wind tunnel (Ref. 4) and in-flight (Ref. 2) noise measurements since the main and tail rotor speeds are nonintegral multiples of each other.

Similar methods have been adapted to the source separation of ground-based measurements of helicopter noise. Because the helicopter is in motion relative to the observers, the measurements are not stationary. However, the ground-based acoustic signals can be transformed into a quasi-stationary measurement (comparable to an observer traveling with the vehicle) using a time-domain de-Dopplerization method (Refs. 5, 6). The idea of combining de-Dopplerization with rotor harmonic averaging for source separation was first explored by Babkin (Ref. 7), but accuracy was limited by fluctuations in the rotor speed. Greenwood and Schmitz (Ref. 8) later inferred the rotor speed from the measured acoustic signal and were able to separate the main and tail rotor noise components. However, phase variations in BVI noise caused the impulses to get averaged out of the signal. BVI could be retained through a phase correction process, but only at the expense of other noise sources. Amplitude variations were still averaged out, leading to an incomplete extraction of the tonal noise.

This shortcoming was addressed by Olsman (Ref. 9) using a modified Fourier transform with time-variant Fourier coefficients. In order to extract the time history of harmonic noise, Hermite B-splines were used to approximate the time-variant coefficients of the Fourier transform, enabling the capture of the nonperiodic components during non-steady-state operating conditions. It was also demonstrated that the nonperiodic and nonstationary signals are captured accurately by the modified Fourier technique. However, due to the complexity of the Hermite spline knots required to accurately model the unsteady changes, quasi-periodic harmonics, and impulsive BVI variations were not extracted. Instead, before applying the modified Fourier transform, BVI noise was extracted using a wavelet-based nonlinear filter developed by Stephenson et al. (Ref. 10). However, this BVI extraction method requires a prioi estimation of the frequency and amplitude of BVI impulses.

An alternative to harmonic averaging is the Vold–Kalman (V-K) order tracking filter (Ref. 11). Stephens and Vold (Ref. 12) used the V-K filter to process open rotor acoustic data from a wind tunnel and also showed that the technique is robust for separating harmonic and broadband noise where conventional averaging methods have limitations. To understand the approach and takeoff noise, Stephens and Vold used the filter to track the highest amplitude forward and aft rotor tones and extract the narrowband random noise. An advantage of the source separation process over conventional techniques is that the phase and amplitude of the harmonic noise are preserved throughout the process. Additionally, unlike harmonic averaging, this method may be used to separate the noise of rotors that are operating at nearly identical but varying frequencies. As such, this approach has the potential to separate the noise of multirotor UAS and AAM vehicles. However, this method has yet to be applied to ground-based measurements of aircraft noise.

Technical Approach

A new approach to rotorcraft noise source separation is developed in this paper based on the V-K order tracking approach. The source separation process is comprised of two main steps. First, the measured acoustic signals are transformed into a stationary reference frame using time-domain de-Dopplerization. Second, the de-Dopplerized data are processed using the V-K filter to separate the main rotor, tail rotor, and residual (i.e., non-rotor-harmonic) components. An overview of the source separation process follows:

De-Dopplerization

Since the method developed in this paper is applied to acoustic measurements of a helicopter collected using ground-based observers, de-Dopplerization is necessary to correct the frequency shift in the signals. The Doppler effect must be removed from the data because the tones become blurred due to the frequency shift in the measured signals (Ref. 5). A time-domain de-Dopplerization procedure was chosen to avoid spectral smearing of the tones over time. This process requires accurate time and position tracking data of the vehicle to calculate the propagation time delay to each microphone, relating the time of observation to the time of emission. Using this information, the measured acoustic signals can be resampled with respect to the emission time by interpolating the pressure amplitude. This process is equivalent to transforming the acoustic signals from a ground-based observer to an observer moving with the aircraft and removing the Doppler frequency shift from the signal. The de-Dopplerization method used in this paper is similar to that used by Greenwood and Schmitz (Ref. 8) but uses higher-order interpolation (Ref. 13) to limit high-frequency distortion.

The relationship between observer times and emission times is given by

$$t_o = t - \frac{r(\tau) - r_o}{a_0} \tag{1}$$

where $r(\tau)$ is the position of the rotorcraft at the time of emission, τ, and t_0 and r_0 are the time and distance offsets of the de-Dopplerized location with respect to the noise source. Since the propagation distance at the time of emission, $r(\tau)$, is known, the signal amplitudes can also be normalized to the virtual microphone location at the same time by correcting

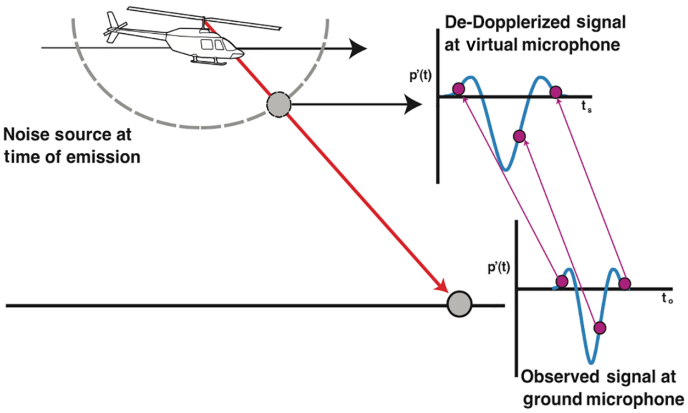

Fig. 1. De-Dopplerization of ground-based microphone signals to a fixed observer with the moving rotorcraft (reproduced from Ref. 8).

for spherical spreading, that is,

$$p_o(t_0) = p(\tau)\frac{r(\tau)}{r_0} \tag{2}$$

Figure 1 represents the de-Dopplerization procedure to transform the signals to a moving observer fixed in the frame of reference of the rotorcraft. For the rotorcraft, the noise is assumed to be originating from a compact source at the rotor hub and the emission angles are calculated based on the observer locations. The signal amplitude, p, was normalized to a fixed distance, r_0, of 100 ft from the source, assuming spherical spreading. No corrections were applied to account for atmospheric absorption. Straight-ray propagation was assumed in the de-Dopplerization process due to good weather conditions and short propagation distances during the flight test.

Vold–Kalman filter

The V-K filter works based on the principle of Wold decomposition (Eq. (3)), where the signal is decomposed into its deterministic and nondeterministic components. Vold developed this smoothing filter based on the Kalman filtering technique (Ref. 14) to approximate the unknown amplitudes of harmonics at known frequencies from a convoluted signal with harmonic and broadband noise. This paper uses the third-generation multishaft V-K filter. The main advantage of the multishaft implementation is that it can extract the interaction tones more accurately than the single-shaft filter (Ref. 12). An overview of the theoretical foundations of the filter based on Ref. 12 is as follows:

The deterministic part $x(t)$ of the signal $y(t)$ is composed of the harmonic components. The nondeterministic part $v(t)$ is assumed to be mostly broadband noise.

$$y(t) = x(t) + v(t) \tag{3}$$

Therefore, the periodic components of interest can be characterized as the deterministic component $x(t)$ with unknown amplitudes occurring at known frequencies. An accurate measurement of rotor speed is required. Using the RPM measurement, a phasor $P(t)$ is constructed with the known blade passing frequency (BPF) of the rotors.

$$P(t) = \exp(2\pi itk\omega(t)) \tag{4}$$

In Eq. (5), $x(t)$ groups together all the known harmonic components of the signal occurring at frequencies $\omega(t)$. These are the orders that will be extracted from the signal using the measured (or inferred) time-varying rotational speed of the rotor, $\omega(t)$.

$$x(t) = \sum_{k\in K} A(t) * P(t) \tag{5}$$

There are two major components in the formulation of the system of equations in the filter; the *structural equation* and the *data equation*. Equation (6) is the *structural equation* of the filter, it forces the amplitudes of the extracted signal to be smooth.

$$\nabla^q A(t) = \epsilon(t) \tag{6}$$

where $\epsilon(t)$ is the nondeterministic term and q is the order of the filter, usually chosen to be 2 or 3 in this paper.

The term ∇^q expands out with the coefficients from Pascal's triangle as shown below for filter orders of 1–3.

$$\begin{aligned}
\nabla A(t) &= A(t+1) - A(t) \\
\nabla^2 A(t) &= A(t+2) - 2A(t+1) + A(t) \\
\nabla^3 A(t) &= A(t+3) - 3A(t+2) + 3A(t+1) - A(t)
\end{aligned} \tag{7}$$

The *data equation* is given in Eq. (8), which ensures that the extracted signal is closely related to the measured tachometer RPM through the complex phasor, $P(t)$. Equation (8) is obtained by substituting Eq. (5) into Eq. (3).

$$v(t) + \sum_{k\in K} A(t)P(t) = y(t) \tag{8}$$

To solve for the complex envelope $A(t)$ using Eqs. (6) and (8), a weighting factor $w(t)$ is chosen based on the bandwidth to minimize the nondeterministic terms, that is, such that $\epsilon(t)$ and $v(t)$ are negligible ($\cong 0$). Therefore,

$$w(t)\nabla^q A(t) \cong 0 \tag{9}$$

$$\sum_{k\in K} A(t)P(t) \cong y(t) \tag{10}$$

where the weighting factor $w(t)$ is calculated using the bandwidth, bw in Eq. (11) as follows:

$$w(t) = \sqrt{\frac{\sqrt{2}-1}{(2(1-\cos(2\pi bw)))^q}} \tag{11}$$

Equations (9) and (10) are used to form a linear system of equations (Eq. (12)) to solve for the complex envelope $A(t)$.

$$\begin{bmatrix} W * \nabla \\ P \end{bmatrix} * A = \begin{bmatrix} 0 \\ Y \end{bmatrix} \tag{12}$$

Here W is a diagonal matrix with the weighting factors, ∇, P are matrices of coefficients and phasor, A is a column vector of the pressure amplitude envelope, and Y is the vector of the measured signal.

The system of equations in Eq. (12) can be solved as a linear least squares problem, typically using well-known solvers, such as Cholesky decomposition, preconditioned conjugate gradient (PCG) algorithm, or an lower-upper (LU) decomposition. In this paper, a Cholesky decomposition was used to solve the system in order to minimize the number of numerical operations. By contrast, Ref. 12 uses a QR decomposition where unitary matrix Q is chosen to reduce the left-hand side of Eq. (12) to an upper triangular matrix. This requires more arithmetic operations than the Cholesky decomposition but enables the V-K filter extraction with narrower bandwidths. In the flight-test data used for paper, the main rotor and tail rotor BPFs are generally far apart; therefore, the Cholesky decomposition is used in this paper with no loss of solution accuracy

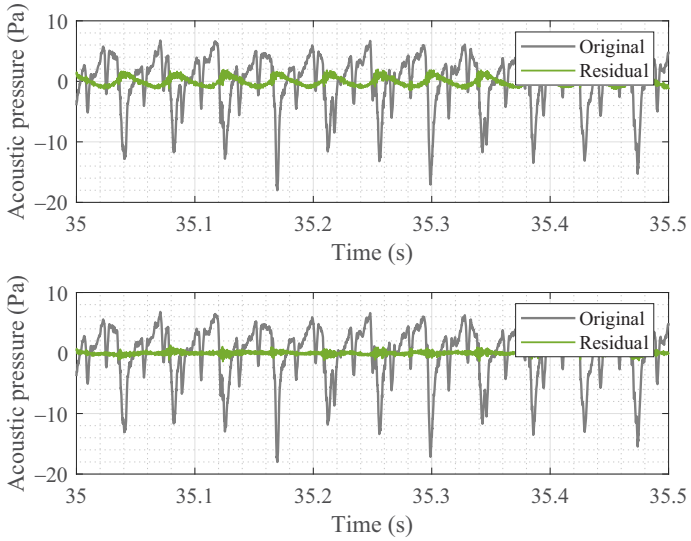

Fig. 2. Original signal and residual signal after extraction for a level flight condition with two different bandwidths: constant bandwidth (top) and proportional bandwidth (bottom).

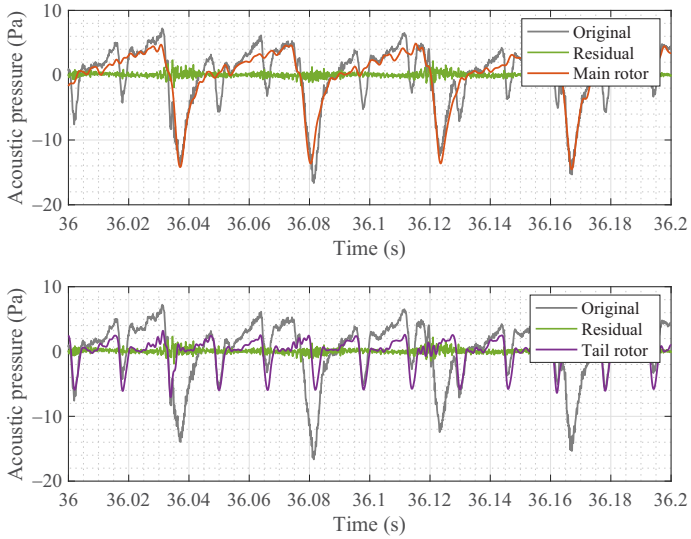

Fig. 3. Extracted time domain pulses of separated signals for a level flight-test case at azimuth 180° and elevation −10°.

in the extracted pressure envelopes. For multirotor aircraft with similar rotor RPM, the accuracy of the extraction may be improved by instead using a QR decomposition, which would enable a narrower bandwidth to be used, albeit at a higher computational cost. The complex envelope consists of the pressure amplitudes of all the extracted orders, that is, extracting the signal while preserving the phase and amplitude relationship of the orders. The extracted signals do not have phase bias because this is not a real-time filter. The V-K filter applied in this paper was tuned to have a variable bandwidth proportional to the extracted rotor BPF and its multiples.

Results and Discussion

Extensive acoustic data were collected during the 2011 Army/Bell/NASA flight test with the Bell 430 helicopter (Ref. 15). These data were acquired using multiple ground-based microphone array layouts for both steady-state and maneuvering flight. The flight test consisted of a 27-microphone linear array for steady source noise characterization and a distributed 31-microphone array for maneuver noise. Among the instrumentation was a main rotor shaft encoder which allowed an accurate measurement of the main rotor rotational speed (RPM). The gear ratio was used to infer the tail rotor RPM from the main rotor RPM measurement, and these RPM readings were used to obtain the BPFs for both rotors. Using the onboard differential GPS tracking data, the propagation times were obtained, and the acoustic measurements were de-Dopplerized to transform them into a stationary reference frame, as described previously. Then the V-K filter was used to extract the first 20 harmonics of the main rotor and the first 10 harmonics of the tail rotor BPFs. The nominal BPF of the main rotor was 23 Hz, and the tail rotor was 63 Hz with a gear ratio of 5.4 between the rotors.

Tuning of several parameters for the V-K filter was performed to obtain accurate results from the source separation process. The weighting factor for the structural equation was formulated based on the bandwidth of the filter (Ref. 16); therefore, the convergence of the solution depends on the choice of the bandwidth. Also, accurate extraction of signals is dependent on bandwidth. If the bandwidth is too narrow the filter does not extract all the energy, essentially performing an incomplete extraction. If the bandwidth is too wide, the filter overextracts the noise, that is, the filter tries to find periodicity in broadband noise. The source separation was tuned for flight-test data and a plot showing the effect of bandwidth in the extracted signal is presented in Fig. 2 for a sample microphone signal from a level flight case.

The original signal is the de-Dopplerized acoustic pressure time history of the signal and residual signal is the component that is leftover after extracting the main and tail rotor components. The filter was tuned to extract the first 20 main rotor harmonics with a filter order of 2, and only the bandwidth is varied between the top plot and the bottom plot in Fig. 2. In the top plot, the bandwidth is set to a constant 30 Hz for all orders and signals; the residual signal has some amplitude modulation, possibly due to incomplete extraction of lower harmonics. In the bottom plot, the bandwidth is proportional and is set to 10% of RPM with a maximum of 25 Hz; the residual signal was smaller, and there is no visible amplitude modulation resulting in an effective extraction.

Level flight case

The source separation process was first applied to a level flight case with 80 kt indicated airspeed. The extracted pressure time histories of the main and tail rotors are presented along with the original and residual signals. The residual signal is obtained by subtracting the time-domain extracted signals from the original acoustic signal. These signals are shown for several main rotor blade passages in Fig. 3. For clarity, the extracted tail rotor signal is omitted from the top plots and the main rotor signal from the lower plots, although both main and tail rotor orders are simultaneously extracted.

There is a clear distinction in the shape of the extracted pulses, which are representative of the main and tail rotor noise of this helicopter. Looking across the larger timescale, small variations in the amplitude and shape of the main and tail rotor pulses can be clearly observed. The residual component primarily contains broadband noise, and the amplitude is significantly lower compared to the extracted main rotor and tail rotor signals.

Figure 4 shows the corresponding power spectrum for the extracted signals. A clean separation of main and tail rotor tones is achieved, even when the harmonics are close to each other. The broadband residual signal does not contribute significantly to the sound pressure levels, and the

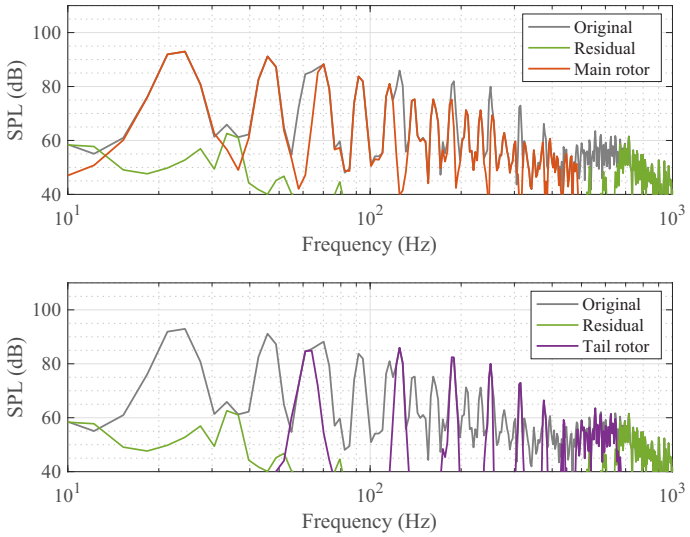

Fig. 4. Extracted frequency spectra of separated signals for an 80-kt level flight-test case at azimuth 180° and elevation −10°.

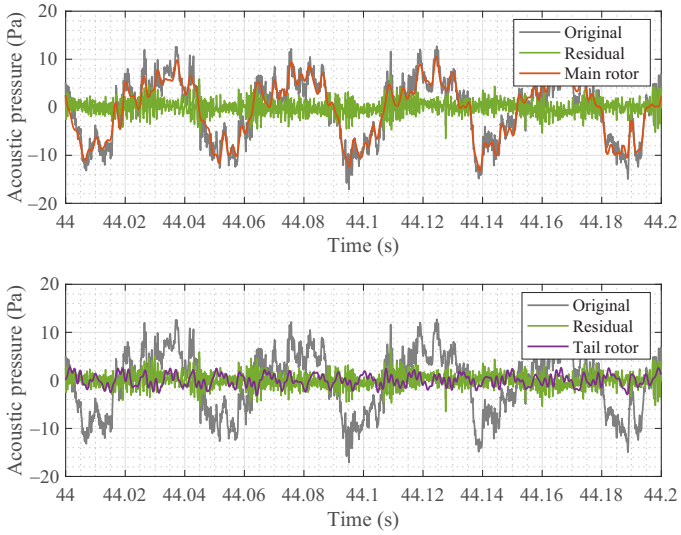

Fig. 6. Extracted time domain pulses of separated signals for an 80-kt level flight-test case at azimuth 140° and elevation −30°.

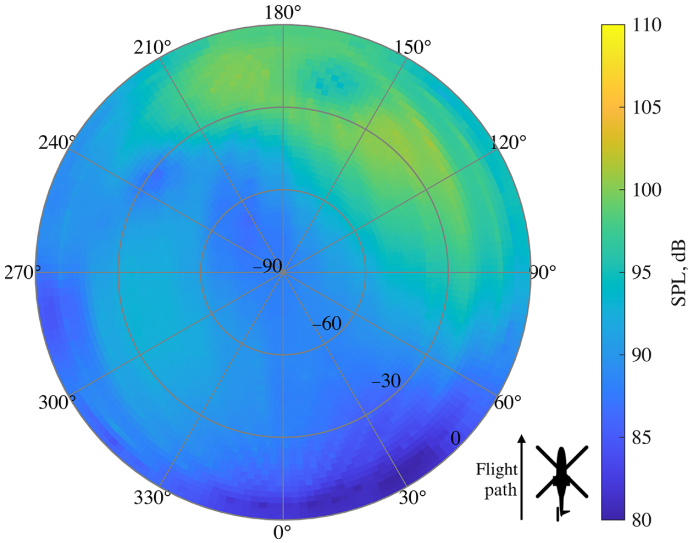

Fig. 5. Noise emission hemisphere of the main rotor for an 80-kt level flight-test case.

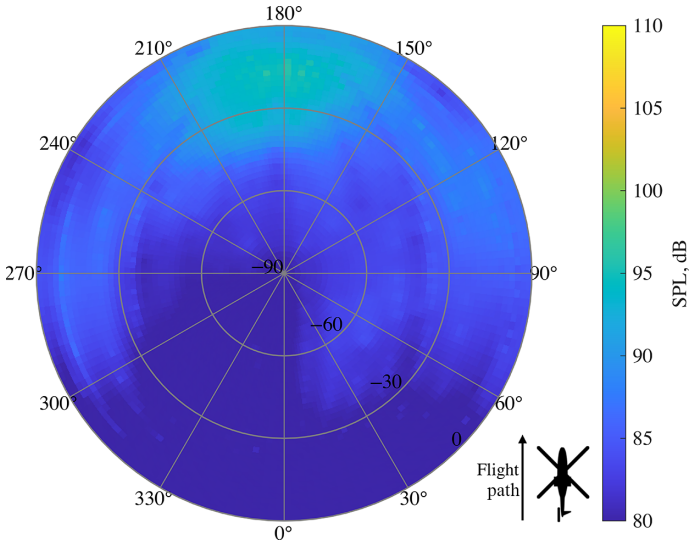

Fig. 7. Noise emission hemisphere of tail rotor for an 80-kt level flight-test case.

magnitude is more than 10 dB below the tones across the frequency range of the extraction.

The extracted data from all the microphones were used to populate a noise hemisphere to visualize the directivity of the individual components. As mentioned in the previous section, the de-Dopplerized acoustic signals were normalized to a 100-ft distance, forming a hemisphere of data around the rotor. All the noise hemispheres in this paper are processed using the raw separated data without any smoothing applied to the noise levels, so as to highlight any variations in time and directionality of the sources. The sound pressure level (SPL) along the microphone tracks on a hemisphere was interpolated using Shepard's inverse distance weighting method (Ref. 17) to a set of regularly spaced points in spherical coordinates and were then plotted on a hemisphere. The extracted main rotor noise hemisphere is presented in Fig. 5 using a stereographic projection. Azimuth angles are plotted around the perimeter, with 180° azimuth representing the front of the helicopter. Elevation angles are plotted with respect to the horizon, ranging from 0° in the horizon to −90° directly below the helicopter. Higher main rotor noise levels are seen both towards the advancing side of the rotor and directly in front of the vehicle.

The extracted pulses shown in Fig. 6 correspond to the noise "hotspot" near an elevation angle of 140° in Fig. 5. The extracted main rotor noise signal features a large amplitude acoustic waveform characteristic of lower harmonic loading noise, with some additional low-amplitude higher harmonic content occurring at multiples of the main rotor blade passing period.

Figure 7 shows the tail rotor extracted noise hemisphere. Here, the noise of the tail rotor reaches a maximum directly ahead of the helicopter, at an azimuth angle of 180°. Examining the spectral data shown in Fig. 4, the noise levels of the extracted tail rotor harmonics are 15–20 dB greater than residual at all the blade passage frequencies.

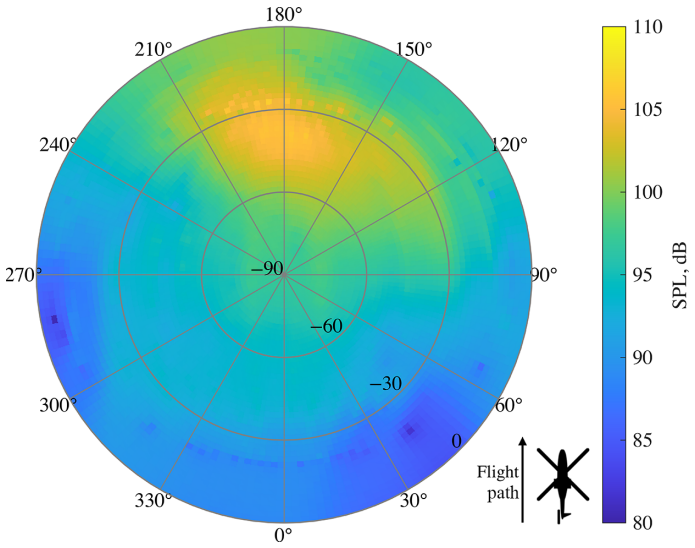

Fig. 8. Noise emission hemisphere of the main rotor for an approach/descent test case.

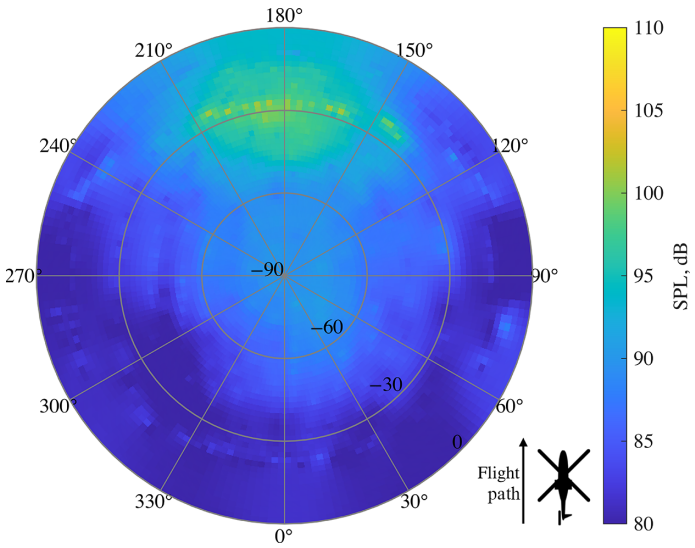

Fig. 9. Noise emission hemisphere of tail rotor for an approach/descent test case.

Approach/descent case

Next, a descent case is analyzed to evaluate the ability of the noise separation approach to extract BVI noise. The selected descent condition has an indicated airspeed of 80 kt and a flight path angle of −6° relative to the horizon. Figure 8 shows the extracted main rotor noise levels plotted on a hemisphere, following the same process as described for the level flight case. A strong noise "hotspot" can be observed radiating ahead of the vehicle for this flight condition.

The tail rotor noise hemisphere for the approach case is shown in Fig. 9. The directivity of the extracted tail rotor noise is similar to the directivity of the tail rotor from level flight seen previously in Fig. 7. This is expected because much of the increase in noise during approach is associated with the main rotor BVI, and so the noise of tail rotor is not expected to vary much from the level flight case at the same airspeed.

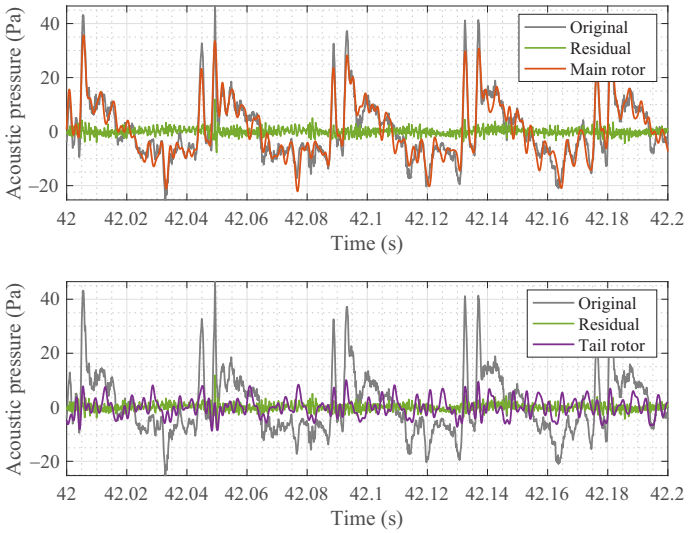

Fig. 10. Extracted time domain pulses of separated signals for an approach/descent test case at azimuth 170° and elevation −50°.

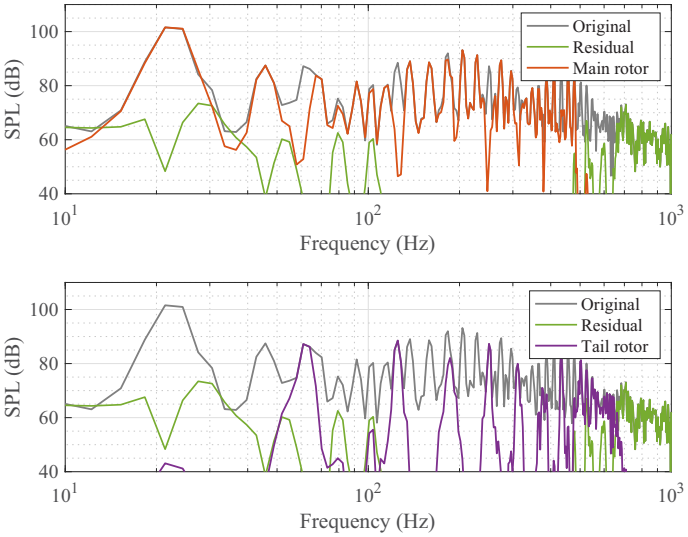

Fig. 11. Extracted frequency spectra of separated signals for an approach/descent test case at azimuth 170° and elevation −50°.

Figure 10 shows the extracted signals for this case at an azimuth of 170° and elevation of −50°. This location was chosen on the hemisphere because it passes through the noise "hotspot" with higher noise levels caused by impulsive BVI events in this test case. There is a clear difference in the shape of the main rotor pulses as compared to the level flight case in Fig. 3. The descending flight case has strong impulsive spikes in amplitude at the blade passage frequency of the main rotor characteristic of BVI noise. At these peaks, small quantities of energy are misinterpreted and extracted as tail rotor components by the source separation process, since the amplitude of the main rotor noise is much greater than that of the tail rotor for this flight condition and in the radiating direction.

The tail rotor pulse seen in the bottom plot features pulses that occur at the tail rotor blade passing period and are similar in shape to those observed in level flight, shown previously in Fig. 3.

The spectra of the extracted main and tail rotors are presented in the top and bottom plots of Fig. 11 respectively. The tonal peaks of the main

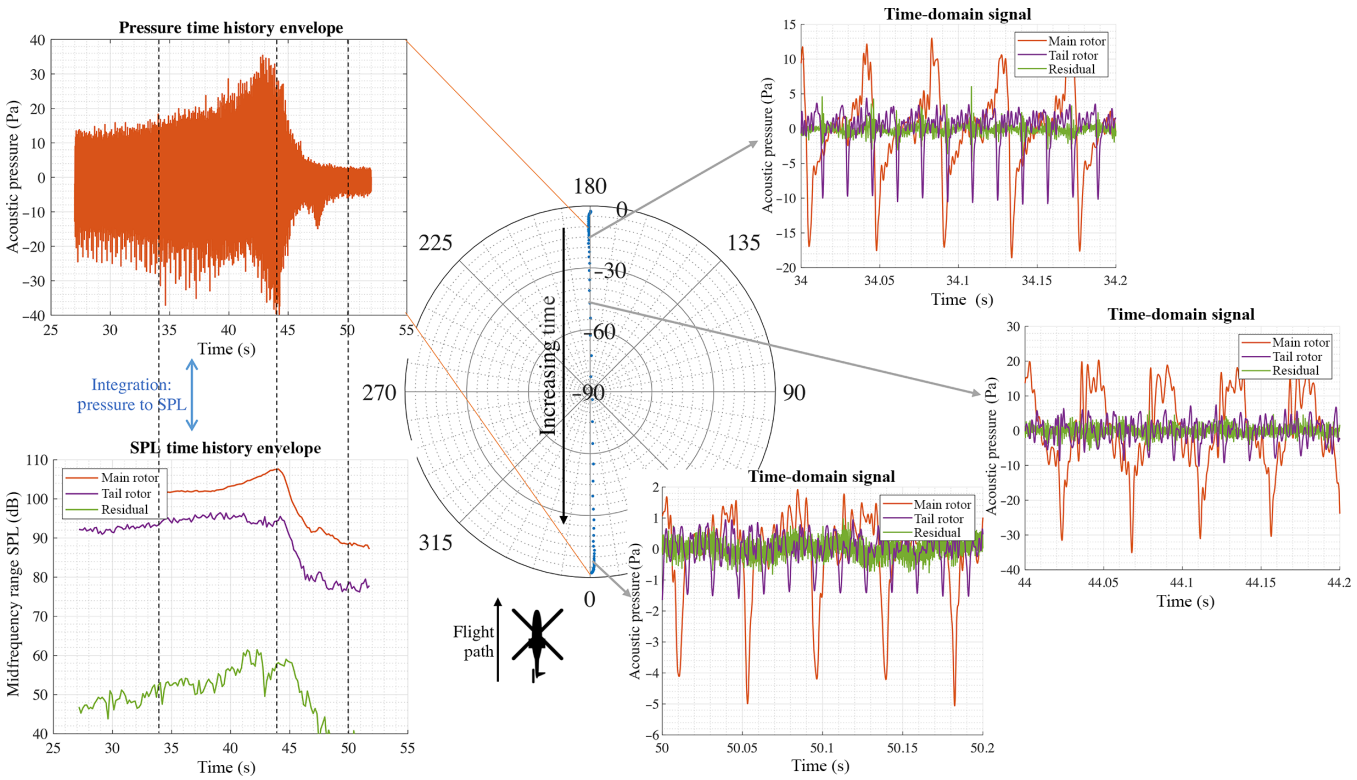

Fig. 12. Acoustic pressure envelope and midfrequency SPL time history for extracted signals along a microphone track with extracted signals on a hemisphere for an approach/descent case.

rotor correspond well in magnitude and frequency to the peaks from the original signal that occur at the first 20 harmonics of the main rotor. While the energy of the extracted harmonic components agrees well in the frequency domain, the extracted signal appears to have smoothed out the peak-to-peak amplitude of the BVI impulses in the time domain, as shown in Fig. 10. Additional tuning of the filter, including the use of higher main rotor orders, may be required to fully resolve these impulsive peaks.

The residual signal consists of a broadband component with a slightly higher amplitude than level flight. This is possibly due to the impulsive noise at higher harmonics and leftover harmonic energy from the extraction. It is also possible that the increased amplitude of modulated broadband noise is associated with blade–wake interaction. In either case, is clear from Fig. 11 that any bleed-through to the broadband component does not significantly change the magnitude of tonal peaks at multiples of the BPF of either extracted rotor components.

The composite plot shown in Fig. 12 shows the extracted components at several emission angles "traced" by a microphone under the helicopter during the flyover. This highlights the advantages of the source separation method where effective extraction is performed with continually changing noise sources along the flight path on a noise hemisphere. In Fig. 12, the pressure time history envelope of the original signal is plotted on the top left plot and a similar SPL envelope for the same time scale is plotted in the bottom left with the integrated SPLs at the midfrequency range (between 4th and 20th main rotor shaft orders) of the separated signals (main rotor, tail rotor, and residual). This frequency range was chosen in order to highlight the ability of the source separation approach to extract BVI noise, which is impulsive and often highly variable over time. Note that during the approach, the main rotor SPL increases by about 10 dB as the aircraft approaches the microphone, whereas the tail rotor component remains relatively constant over the same period of time. The SPL of all the components drops as the aircraft passes over the microphone. The microphone trace is plotted on a hemisphere in the center. Three pressure time history plots of extracted signals are plotted for times of 34–34.2 s, 44–44.2 s, and 50–50.2 s along the microphone trace. These are distinctive points in the hemisphere, each of which is characterized by a different composition of noise sources. Note that the vertical axis varies between each of the three pressure time history plots, due to the large variation in amplitudes associated with the three selected emission angles.

The first signal shown begins at 34 s, corresponding to a location on the hemisphere with an azimuth of 180° and elevation of −15°. Thickness noise, both that of the main rotor and the tail rotor, dominates this region because thickness noise radiates most strongly in the plane of the rotors in the direction of travel. The second signal beings at 44 s; this is at azimuth 180° and elevation −45°. Here, the observer is out of the plane of the main rotor and loading noise is dominant. The pulse shapes of the main rotor show strong BVI impulses with a negative peak, indicative of retreating side BVI. The tail rotor component retains the negative peaks associated with thickness noise at the blade passing period of the tail rotor noise. The third signal begins at 50 s at an azimuth of 360° and elevation of −7°. In this direction, the broadband noise is relatively more significant since the extracted main and tail rotor noise levels are much lower in directions below and behind the helicopter than ahead of it.

Maneuver case

Finally, a pitch-up maneuver is presented in this section to examine the applicability of the method to nonsteady flight conditions. The maneuver is a cyclic pitch-up case initiated at an indicated airspeed of 60 kt. Since the vehicle and its radiated noise are not stationary throughout the maneuver, it is not possible to construct a meaningful acoustic

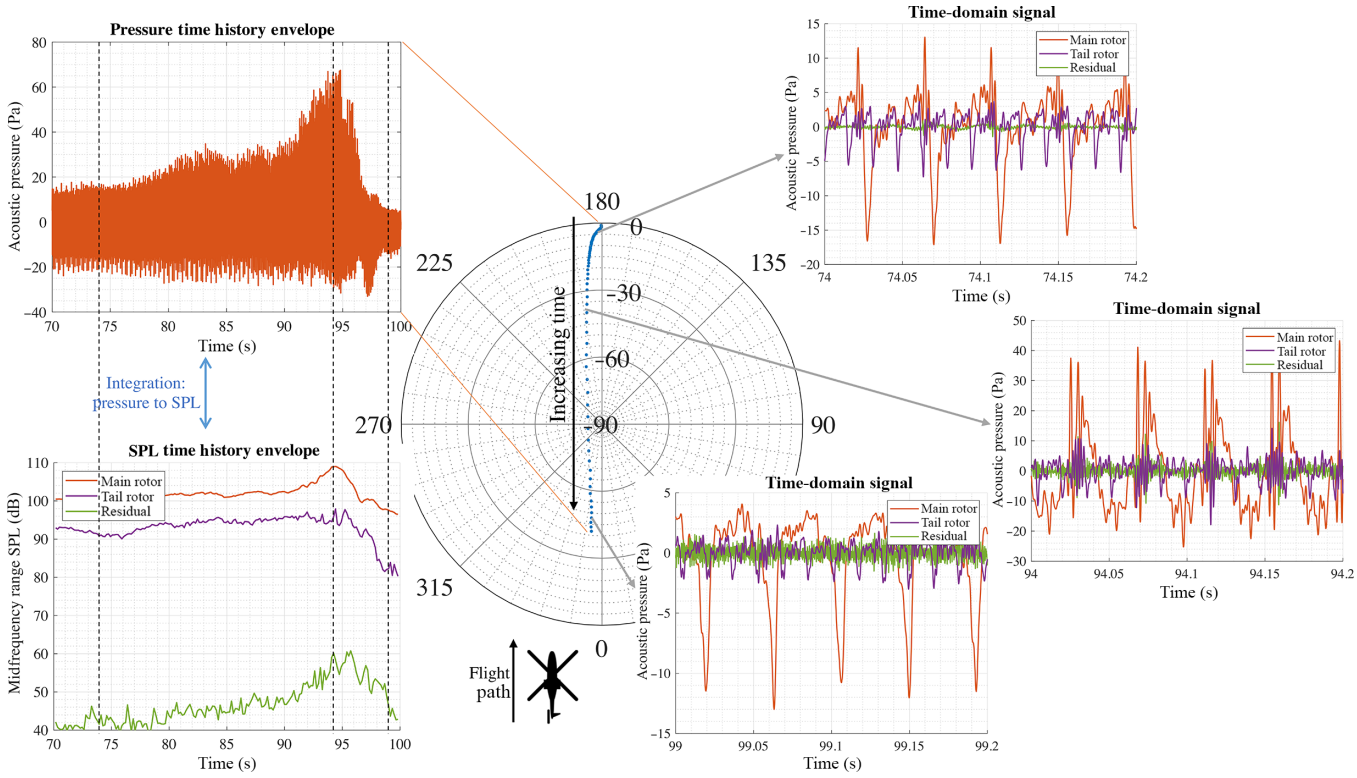

Fig. 13. Acoustic pressure envelope and midfrequency SPL time history for extracted signals along a microphone track with extracted signals on a hemisphere for a cyclic pitch-up maneuver flight case.

hemisphere from the measured data. Instead, the variation in measured noise with time and direction is shown using a composite plot in Fig. 13. The path traced by the selected microphone is shown on a spherical surface in the center of the plot.

The top left plot contains the envelope of pressure time history of the original signal. The corresponding SPL time history is shown for the same timescale in the bottom left plot for extracted main rotor, tail rotor, and residual components. The presented SPL plots are integrated over a midfrequency range from 90 to 470 Hz, which is between the 4th harmonic and 20th harmonic of the main rotor and was targeted to isolate BVI noise levels from the extracted signals. Throughout the maneuver, the midfrequency main rotor SPL is higher than the tail rotor SPL. Both tonal components are significantly higher than the residual. However, the variation in time is significantly different for all three components. The tonal component SPL is much greater ahead of the helicopter than towards the rear of the vehicle. The tail rotor SPL stays relatively constant for most of the maneuver, decreasing only after the helicopter has completed the maneuver and has passed over the microphone. Similar to the approach case, the main rotor SPL increases by approximately 10 dB as the aircraft approaches the microphone during the maneuver. The residual signal peaks occur after the peaks of both the extracted tonal components and are biased towards the rear of the vehicle.

The extracted signal of the main rotor is presented along with extracted tail rotor and is plotted at three different time instants to highlight the different noise sources that occur during a maneuver. The first time window is from 74 to 74.2 s near an azimuth 180° and elevation from 0° to −30°. The extracted main rotor signal shows the prominent negative acoustic peaks associated with thickness noise, although there are also positive impulses associated with BVI during this stage of flight. The second signal shown is from 94 to 94.2 s which is located at azimuth 180° and elevation −45°. The pulse shape of the extracted noise in this direction is characteristic of strong BVI noise with two BVI impulses occurring during each rotor blade passage. The amplitude of the signal is higher, and there is a corresponding rise in the main rotor levels in SPL time history shown in the bottom left plot. Note once again that the pressure time history scale has been changed to better resolve the details of the pulses. The third signal is from 99 to 99.2 s and is located at azimuth 350° and elevation −45°. The extracted main rotor noise shows characteristic thickness noise pulses in the aft direction.

The tail rotor noise is relatively constant throughout the maneuver. Examining the waveforms shows the characteristic negative peaks associated with tail rotor thickness noise, which are not expected to vary much with changes in the rotor-operating condition. Additionally, the microphone remains in the plane of the tail rotor throughout the maneuver, explaining the relative lack of variation in the extracted tail rotor component.

Conclusions

The paper developed a source separation approach based on the V-K filtering technique and applied it to flight-test data. Since the data were from ground-based microphones, a de-Dopplerization step was used to transform the signals into a virtual observer at a fixed distance from the vehicle in the moving frame of reference. The de-Dopplerization step was the first step in the twofold procedure with the V-K filter as the second step. A few representative cases were presented to demonstrate the capabilities and/or limitations of the source separation process. Since the order tracking filter preserves the phase and amplitude relationship of the extracted components, both time-domain and frequency-domain analysis of the extracted components can be performed. This is a major advantage over other conventional source separation techniques, especially in cases where radiated noise varies over time.

The method was first applied to a level flight condition for a Bell 430 helicopter. Main rotor, tail rotor, and broadband components were

extracted. As expected, thickness noise was most significant ahead of the helicopter, and the loading noise was dominant out of the plane of the rotor. The extraction method was shown to accurately account for all acoustic energy between the three components. Next, an approach case was presented with high levels of impulsive BVI noise. The method was effective in extracting the BVI noise. There was some "bleed-through" of the main rotor impulsive noise into the tail rotor signal since the BVI pulses occupy a similar frequency range but are 8–10 times larger in amplitude. Finally, the process was applied to a cyclic pitch-up maneuver case, where the noise at the source varied over time. A clean extraction of main and tail rotor signals was achieved for this case.

To the authors' knowledge, this is the first time a V-K filter has been used to analyze the noise of a moving helicopter. This technique can be used to separate and analyze the time-varying components of rotor noise, both to understand maneuvering flight noise and to assess the time variation of components during nominal steady flight. Building on other work conducted in a stationary frame, this method may also be extended to separate the noise generated by different rotors on a multirotor UAS and UAM vehicle by closely tracking the changes in RPM between the different rotors.

Acknowledgments

This research was funded by the U.S. Federal Aviation Administration (FAA) Office of Environment and Energy (AEE) through ASCENT, the FAA Center of Excellence for Alternative Jet Fuels and the Environment, Project 77 through FAA Award Number 13-C-AJFE-PSU Amendment No. 67 managed by Dr. Hua (Bill) He of AEE. Any opinions, findings, conclusions, or recommendations expressed in this material are those of the authors and do not necessarily reflect the views of the FAA.

References

[1]Boxwell, D. A., Schmitz, F. H., Splettstoesser, W. R., and Schultz, K. J., "Helicopter Model RotorBlade Vortex Interaction Impulsive Noise: Scalability and Parametric Variations," *Journal of the American Helicopter Society*, Vol. 32, (1), October 1987, pp. 3–12, DOI: 10.4050/JAHS.32.1.3.

[2]Sargent, D. C., Schmitz, F. H., and Sim, B. W., "In-Flight Array Measurements of Tail Rotor Harmonic Noise," *Journal of the American Helicopter Society*, **55**, 012006 (2010), DOI: 10.4050/JAHS.55.012006.

[3]Boxwell, D. A., Schmitz, F. H., Splettstoesser, W. R., Schultz, K. J., Lewy, S., and Caplot, M., "A Comparison of the Acoustic and Aerodynamic Measurements of Model Rotor Tested in Two Anechoic Wind Tunnels," NASA TM 88364, 1986.

[4]Yin, J., van der Wall, B. G., and Oerlemans, S., "Acoustic Wind Tunnel Tests on Helicopter Tail Rotor Noise (HeliNOVI)," *Journal of the American Helicopter Society*, Vol. 53, (3), 2008, pp. 226–239, DOI: 10.4050/JAHS.53.226.

[5]Howell, G. P., Bradley, A. J., McCormick, M. A., and Brown, J. D., "De-Dopplerization and Acoustic Imaging of Aircraft Flyover Noise Measurements," *Journal of Sound and Vibration*, Vol. 105, (1), 1986, pp. 151–167, DOI: 10.1016/0022-460X(86)90227-0.

[6]Kelly, J. J., and Wilson, M. R., "De-Dopplerization of Aircraft Acoustic Signals," *Journal of Aircraft*, Vol. 32, (5), 1995, pp. 1012–1017, DOI: 10.2514/3.46830.

[7]Babkin, A. S., "Signal Restoration of Non-Stationary Acoustic Signals in the Time Domain," NASA CR 181627, 1988.

[8]Greenwood, E., and Schmitz, F. H., "Separation of Main and Tail Rotor Noise from Ground-Based Acoustic Measurements," *Journal of Aircraft*, Vol. 51, (2), 2014, pp. 464–472, DOI: 10.2514/1.C032046.

[9]Olsman, W. F. J., "Method for the Extraction of Helicopter Main and Tail Rotor Noise," *Journal of Aircraft*, Vol. 55, (2), 2018, pp. 805–816, DOI: 10.2514/1.C034525.

[10]Stephenson, J. H., Tinney, C. E., Greenwood, E., and Watts, M. E., "Time Frequency Analysis of Sound from a Maneuvering Rotorcraft," *Journal of Sound and Vibration*, Vol. 333, (21), 2014, pp. 5324–5339, DOI: 10.1016/j.jsv.2014.05.018.

[11]Vold, H., Mains, M., and Blough, J., "Theoretical Foundations for High Performance Order Tracking with the Vold-Kalman Tracking Filter," SAE Technical Paper 972007, 1997, DOI: 10.4271/972007.

[12]Stephens, D. B., and Vold, H., "Order Tracking Signal Processing for Open Rotor Acoustics," *Journal of Sound and Vibration*, Vol. 333, (16), 2014, pp. 3818–3830, DOI: 10.1016/j.jsv.2014.04.005.

[13]Rizzi, S. A., Christian, A. W., and Rafaelof, M., "A Laboratory Method for Assessing Audibility and Localization of Rotorcraft Fly-In Noise" *Journal of the American Helicopter Society*, **64**, 012009 (2019), DOI: 10.4050/JAHS.64.012009.

[14]Kalman, R. E., "A New Approach to Linear Filtering and Prediction Problems," *Journal of Basic Engineering*, Vol. 82, (1), 1960, pp. 35–45, DOI: 10.1115/1.3662552.

[15]Watts, M. E., Greenwood, E., Smith, C. D., Snider, R., and Conner, D. A., "Maneuver Acoustic Flight Test of the Bell 430 Helicopter Data Report," NASA TM 218266, 2014.

[16]Tuma, J., "Setting the Passband Width in the Vold-Kalman Order Tracking Filter," Proceedings of the 12th International Congress on Sound and Vibration, Lisbon, Portugal, July 11–14, 2005.

[17]Shepard, D., "A Two-Dimensional Interpolation Function for Irregularly-Spaced Data," Proceedings of the 1968 23rd ACM National Conference, August 27–29, 1968, DOI: 10.1145/800186.810616.